Quasifission reactions as a probe of nuclear viscosity

J. Velkovska, C. R. Morton,* R. L. McGrath, P. Chung, and I. Diószegi
Department of Physics and Astronomy, State University of New York at Stony Brook, Stony Brook, New York 11794
(Received 27 July 1998)

Fission fragment mass and angular distributions were measured from the ^{64}Ni+ ^{197}Au reaction at 418 MeV and 383 MeV incident energy. A detailed data analysis was performed, using the one-body dissipation theory implemented in the code HICOL. The effect of the window and the wall friction on the experimental observables was investigated. Friction stronger than one body was also considered. The mass and angular distributions were consistent with one-body dissipation. An evaporation code DIFHEAT coupled to HICOL was developed in order to predict reaction time scales required to describe available data on prescission neutron multiplicities. The multiplicity data were again consistent with one-body dissipation. The cross sections for touch, capture and quasifission were also obtained. [S0556-2813(99)05803-3]

PACS number(s): 25.70.Lm, 25.70.Jj, 24.10.−i

I. INTRODUCTION

The mechanism through which energy is dissipated in low energy heavy ion reactions is a topic widely discussed in the last 20 years. The study of deep-inelastic collisions in the 1970s stimulated the development of dissipative theories of nuclear dynamics [1,2]. Following this, the quasifission phenomenon was discovered in the 1980s. As well as fusion-fission, it belongs to the class of the completely damped reactions, where all the initial kinetic energy is dissipated, but depending on the entrance channel, the mass asymmetry degree of freedom may be fully or partially equilibrated [3]. Large mass transfer is achieved in a relatively short time $(2-10\times10^{-21}$ s) [4] and the system quickly reseparates due to the absence of a fission barrier.

In heavy symmetric systems, quasifission is the dominant reaction mechanism. A number of systematic studies done at GSI [4–6] using ^{238}U and ^{208}Pb beams incident on targets ranging from ^{16}O to ^{89}Y have identified the following experimental signatures of quasifission: (i) fragment mass distributions wider than the mass distributions resulting from fusion-fission reactions, (ii) asymmetries in the mass-angle correlations increasing with the target mass, and (iii) angular anisotropies significantly larger than those in fusion-fission reactions.

Because of their unique nature, quasifission reactions can provide a testing ground for different models of dissipative heavy ion collisions. While in fusion-fission reactions the fragment mass distributions are not informative of the reaction dynamics, in quasifission the mass drift towards symmetry is a sensitive probe of the dissipative forces acting between the reaction partners. The asymmetry in the mass-angle correlations, wherever present, is directly related to the time the system spends in the coalesced state, before reseparation. In the GSI measurements it was determined that for all targets heavier than ^{40}Ca the system made less than one turn before reseparating and the turning angle of the intermediate complex was used to extract the dynamical time scale of the reaction. The data analysis found that the relevant friction mechanism is one body in nature and is temperature independent. As a result of these works, the extra-push model parameters were established in a systematic way. They were also used in the development of the one-body dissipation model implemented in Feldmeier's code HICOL [7].

Another experimental approach for determining the reaction time scale is the measurement of prescission neutron multiplicities. This approach is not limited to quasifission reactions, but was also used to deduce fusion-fission time scales [8,9]. When the excitation energy of the coalesced system is high enough, the neutron evaporation times are much shorter than the scission time and, thus, the prescission neutron multiplicity can be used as a clock. The theoretical treatment of the data involves a statistical model code, which is used to predict the prescission neutron lifetimes and to deduce the reaction time. Although the dynamics of the reaction cannot be treated with this model, and a direct comparison with the different dissipation theories has not been done, the quasifission time scales derived from prescission neutron multiplicities are comparable to the results obtained with mass-angle correlations in similar systems and temperature regimes [4–6].

In recent work, Wilczynski and co-workers [10,11] reanalyzed prescission neutron multiplicity data of Hinde *et al.* [8,9] using an evaporation code DYNSEQ coupled to the outputs of HICOL. In that way, the dynamics of the reaction was taken into account. The time scales obtained were an order of magnitude longer than the original results of Hinde *et al.* Surprisingly large values for the dimensionless friction coefficient $\gamma=17-50$ were reported. These were derived after scaling the one-body dissipation in HICOL by a factor $k_s=4-12$. Using this new analysis, and results of the analysis [12] of the GDR γ rays in coincidence with fission for the O+Pb, S+W, Pb reactions [13], the authors claimed to observe strong two-body dissipation setting in at nuclear temperature of about 2 MeV with γ following $1/T^2$ temperature dependence. One-body friction, for comparison, yields $\gamma\sim4$ independent of temperature.

The strength of two-body dissipation is still an open ques-

*Present address: Department of Nuclear Physics, Research School of Physical Sciences and Engineering, Australian National University, Canberra, Act 0200, Australia.

tion in the literature. While most authors find that two-body dissipation is weaker than one body and yields shorter prescission time scales [14,15], there are some theoretical works that predict strong two-body viscosity and long time scales associated with this (e.g., [16]). Such strong dissipation, if present, would influence significantly the quasifission reaction dynamics and the observables associated with it: fragment mass distributions and mass-angle correlations. It is desirable to compare dissipation results deduced from prescission neutron multiplicities and from fragment mass and angular distributions. At present, there are four quasifission reactions in which the prescission neutron multiplicities have been measured [9]. The data set of mass-angle correlations is larger, but until now, there was no measurement of both observables in the same reaction at the same center of mass (c.m.) energy, and hence, the same nuclear temperature.

In this work the mass and angular distributions were measured in the ^{64}Ni+^{197}Au reaction at 418 MeV and 383 MeV laboratory energies. The mass-angle correlations were also constructed. For the first bombarding energy, prescission neutron data exist and a comparison of the two experimental approaches is possible. The second energy was used to investigate the temperature dependence of the friction. With the development of the code HICOL, a detailed analysis of the mass distributions became possible and the relative contribution of the window and the wall friction could be determined from the data. An upper limit to the reaction time, and the friction, was determined by an analysis of the mass-angle correlations using the one-body dissipation model HICOL. An evaporation code DIFHEAT, coupled to HICOL, was developed and applied for analysis of the prescission neutron data published in Ref. [9] and a comparison with Wilczynski's results (obtained with a different code) is presented. The deep inelastic, capture and touch cross sections were also obtained.

II. EXPERIMENT

The experiment was performed at the Stony Brook Nuclear Structure Laboratory, using ^{64}Ni beam from the FN Tandem Van de Graaff and superconducting LINAC accelerators.

The reactions, for which the prescission neutron multiplicities were measured and the two existing interpretations for the reaction times, determined in Refs. [9] and [10] are given in Table I. To complement the prescission neutron multiplicity data, we measured the mass and angular distributions of the fragments produced from^{64}Ni+^{197}Au at 418 MeV incident energy. Although in this case the discrepancy shown in Table I is mild compared to the ^{64}Ni+^{238}U and ^{40}Ar+^{238}U reactions, the ^{197}Au target was chosen for its lower fissility. The measurements were performed in ''singles'' mode with silicon surface barrier detectors (SSB's) and the event reconstruction was done assuming binary fission.

The experimental layout in the 2.4 m diameter ''BigMac'' scattering chamber is shown in Fig. 1. Eight large area SSB's (EG&G Ortec BF-028-400-60) were mounted on a movable platform 10° apart located at distances 50 cm and 40 cm from the target. Measurements were done at two positions of the platform, covering from 20° to 90° laboratory angles in the forward position and from 80° to 150° in the backward position. The platform was connected to a cooling system and the detectors were cooled to -10 °C, which allowed over-biasing without damaging the detectors. Operating the SSB's in high field strength was crucial, since this minimizes the pulse-height defect and the plasma delay. For the heavy ions studied in this experiment, the plasma delay time was between 0.2 and 1.5 ns. Corrections were made to compensate for this effect. The pulse-height defects were $E_{\rm phd}=5-25$ MeV. Although systematic studies of the two effects listed above are present in the literature [17,18], the correct mass reconstruction for ions as heavy as the fission fragments measured in this experiment was difficult. An original procedure for mass reconstruction was developed in this work and is discussed in Ref. [19]. In addition, two small area ion-implanted silicon detectors (EG&G Ortec BU-013-25-300) were placed at $\pm 20°$ with respect to the beam axis at a distance 81 cm from the target to monitor the beam quality and for normalization of the measured fission fragment yield to the Rutherford scattering cross section.

TABLE I. Quasifission reactions, prescission neutron multiplicities, and reaction times.

Reaction	$E_{\rm lab}$ (MeV)	$\nu_{\rm pre}$	$\tau_f\times10^{-21}$ s[a]	$\tau_f\times10^{-21}$ s[b]
^{40}Ar+^{238}U	249	3.25±0.2	30±10	$390\pm^{80}_{60}$
^{64}Ni+^{197}Au	418	3.15±0.6	18±9	$80\pm^{55}_{25}$
^{64}Ni+^{208}Pb	418	3.25±0.6	28±10	$70\pm^{35}_{25}$
^{64}Ni+^{238}U	418	4.00±0.8	15±8	$120\pm^{90}_{40}$

[a]From Ref. [9].
[b]From Ref. [10].

The reconstruction of the mass and the energy of the detected fragments requires an energy and absolute time-of-fight (TOF) calibration of the detectors and the subsequent electronics. The energy calibration was done using a ^{228}Th α source and the elastic peak from a 247 MeV ^{64}Ni beam. At the $E_{\rm lab}=418$ MeV energy, additional calibration points from elastic scattering were used for the detectors that were within the reaction grazing angle. The energy resolu-

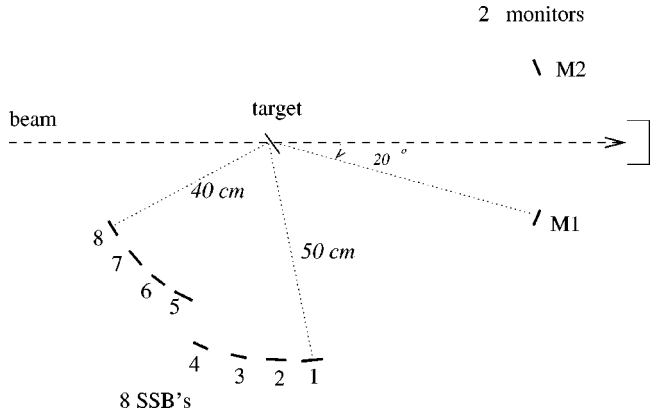

FIG. 1. The experimental layout in the ''BigMac'' scattering chamber.

tion was ~2% for the elastically scattered beam and ~1.2% for α particles. An absolute timing calibration was done using the reference rf signal of the LINAC accelerator and the elastic peak from the 247 MeV run. A thin (100 μg/cm^2) self-supporting Au target was used in the calibration and a 250 μg/cm^2 Au target was chosen for the measurement, compromising between good timing and a reasonably high count rate. The width of the beam pulse at the target was $\leqslant$600 ps full width at half maximum (FWHM). Corrections were made for the plasma delay time of the heavy fragments, and the overall timing resolution for the elastic reaction products measured was $\leqslant$1 ns.

In addition, the relative solid angles of the SSB's and the monitors were calibrated using the Rutherford scattering yield. Several calibration runs at 247 MeV, bracketing in time the higher energy data, were recorded during the course of the experiment.

III. DATA ANALYSIS

A. Mass reconstruction

Two-dimensional (2D) scatter plots energy versus TOF were made for each detector, and the reaction products were separated from the slit scattered beam and low-energy-noise backgrounds by applying 2D gates. An example of such a plot and the gate applied for detector 3, located at 40° in the laboratory system, is shown in Fig. 2(a). The high-energy elastic peak dominates the yield. Quasielastic events are seen at an energy lower than the elastics and with similar TOF. The regions of the deep-inelastic and the quasifission fragments are indicated in the figure. Although the elastic and quasielastic channels are not of interest for the quasifission reaction studied here, these events (wherever present) provided an important check for the mass reconstruction; so they were included in the first step of the data analysis. Later, when only the damped reaction products were studied, total kinetic energy (TKE) versus mass scatter plots were made for each detector and a gate was applied to select the deep-inelastic and quasifission events only. See Fig. 2(b) for θ=40° (lab).

After selecting the events of interest,the mass was reconstructed, as described in Ref. [19], with overall mass resolution better than 10 mass units.

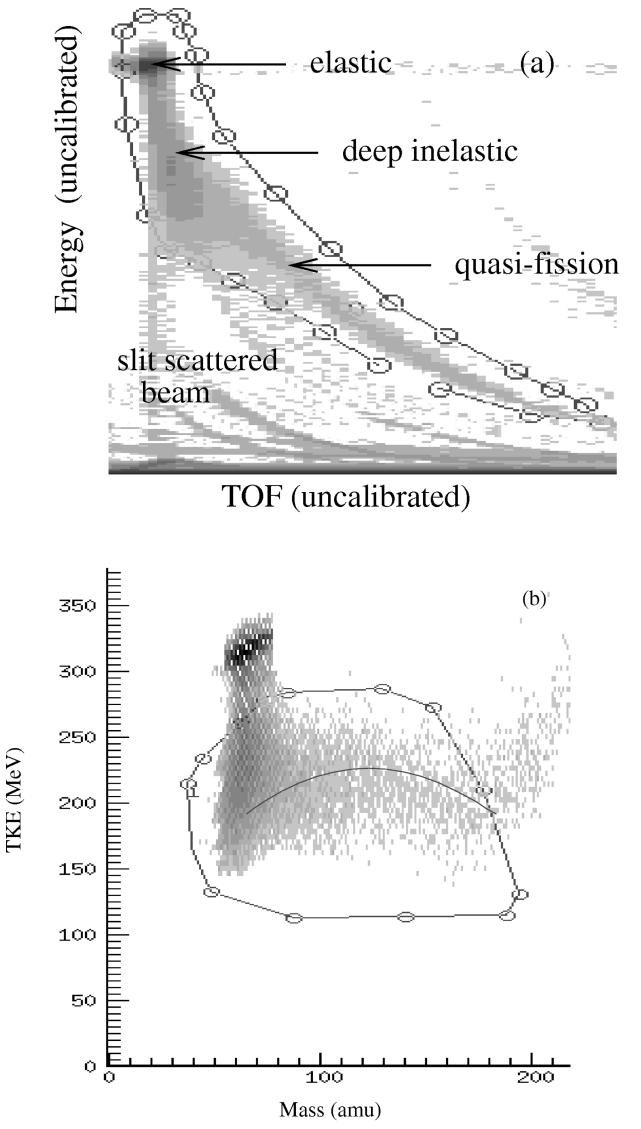

FIG. 2. Scatter plots from detector 3 located at 40° in the laboratory system for E_{lab}=418 MeV. (a) Energy versus TOF (uncalibrated). The ''banana'' gate applied to select the events of interest is shown. (b) TKE (MeV) versus mass (amu). The gate shown separates the quasifission and the deep-inelastic events from the elastic and quasielastic scattering. The line shows Viola systematics TKE.

B. Efficiency simulations

A Monte Carlo simulation program was developed to determine the detection efficiency for each mass at each detector position. Events were generated in the c.m. with flat mass distribution and $d\sigma/d\Omega_{\text{c.m.}}=1/\sin\theta$ (assuming an isotropic distribution in the azimuthal angle θ). The kinetic energy of the fragments was drawn from a Gaussian distribution with parameters determined from the measured TKE distributions, as discussed later. The simulations included energy loss in the target and in the front Au electrode of the detector, pulse-height-defect and plasma delay, electronics energy thresholds, TOF, and velocity cuts. After applying the experimental cuts and the experimental mass reconstruction procedure, the events were transformed back into the c.m. and the ''detected'' yield was compared to the input. The efficiency curves for the two energies studied and for the two positions of the platform holding the detectors are shown in Fig. 3. For small masses, the input angular distribution is recovered from the ''data,'' in the intermediate mass region (A=125–130), the detection efficiency is reduced in the three most backward detector positions, and the heavy fragments (A >150) can only be detected in the forward position of the platform (from 20° to 90° in the laboratory system).

The mass cuts observed in this experiment agree very well with the simulated efficiency curves. This gives confidence that the mass reconstruction in the experimental data was done correctly and, also, that all relevant effects were included in the simulations. Based on the simulated efficiency, a correction to the experimental yield was done for the mass bins in which the efficiency was between 0.5 and 1. For lower efficiencies, the centroid of the fragment kinetic

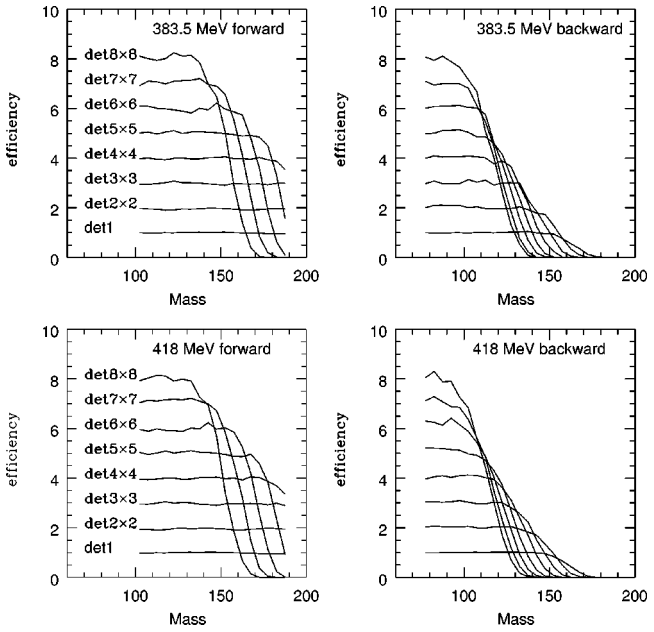

FIG. 3. Efficiency curves for all eight detectors in the two positions of the platform for $E_{\rm lab}=418$ MeV and $E_{\rm lab}=383$ MeV.

energy distribution is not covered; so these data were excluded from the analysis.

IV. RESULTS AND DISCUSSION

A. Fragment mass-TKE distributions

Two-dimensional scatter plots of TKE (in the c.m.) versus mass were generated for each detector. The data were corrected for prescission and postscission neutron emission, using the measured quantities from Ref. [9]: for 418 MeV, $\nu_{\rm pre}=3.15, \nu_{\rm post}=2-5$ depending on the mass of the fragment. For $E_{\rm lab}=383$ MeV, experimental data are not available; so values estimated on the basis of HICOL's predictions for the heat along the trajectory and in each fragment at the scission point were used: $\nu_{\rm pre}=1.5$ and $\nu_{\rm post}=1-3$, increasing with the fragment mass. In Fig. 2(b) an example of TKE-mass scatter plot is shown. The line indicates the Viola-systematics energy. The measured centroids of the TKE distributions agree with Viola systematics and with previous quasifission studies [4–6]. The variance of the distribution, for which systematic data and empirical formulas do not exist, was determined to be ≈15% from the centroid and is again consistent with the measurements in Ref. [6]. The HICOL calculations, discussed later, predict correctly the centroid of the TKE distribution, which shows that the friction mechanism implemented in the code produces the right amount of damping.

B. Fragment angular distributions

1. Experimental results

The energy-integrated cross sections binned in 10 mass units, $d\sigma/d\theta_{\rm c.m.}=2\pi\sin\theta_{\rm c.m.}d\sigma/d\Omega_{\rm c.m.}$, were constructed, after laboratory to c.m. transformation and normalization to the Rutherford scattering yield.

Figures 4 and 5 show the results from the two energies measured. The data for the masses up to the symmetric mass split are shown with solid circles. Above symmetry, only a limited angular range was covered, due to the various factors restricting the measurement and the mass reconstruction. The data obtained in this region were used for a consistency check and are plotted with open points in their complementary mass bins. The error bars shown in the figures represent the statistical errors from the measurement. The data show a significant forward-backward asymmetry typical for short-time scale reactions in which the rotational period of the system is longer than the reaction time. This behavior is consistent with one-body friction.

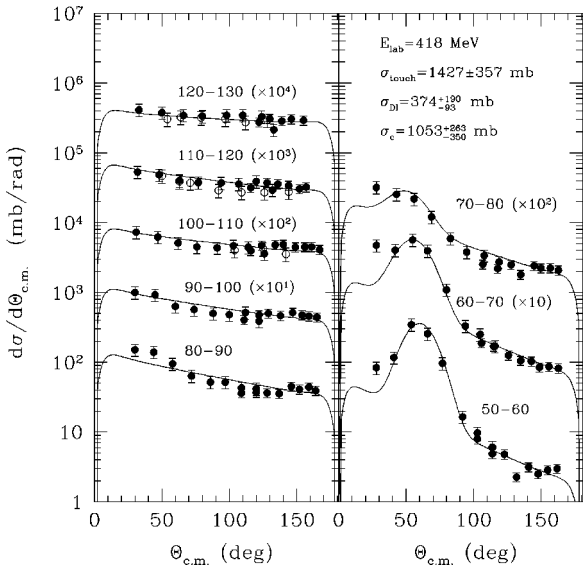

FIG. 4. Fragment angular distributions in bins of 10 mass units from the $E_{\rm lab}=418$ MeV measurement. The fits to the data are described in the text. The values of the measured cross sections are given. The open points come from the measurements in the complementary mass bin with the assumption that binary fission is observed.

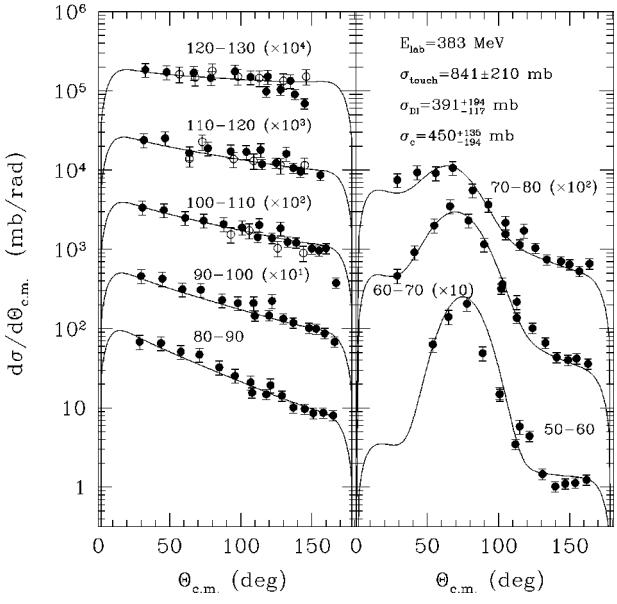

FIG. 5. As per Fig. 4 but for $E_{\rm lab}=383$ MeV.

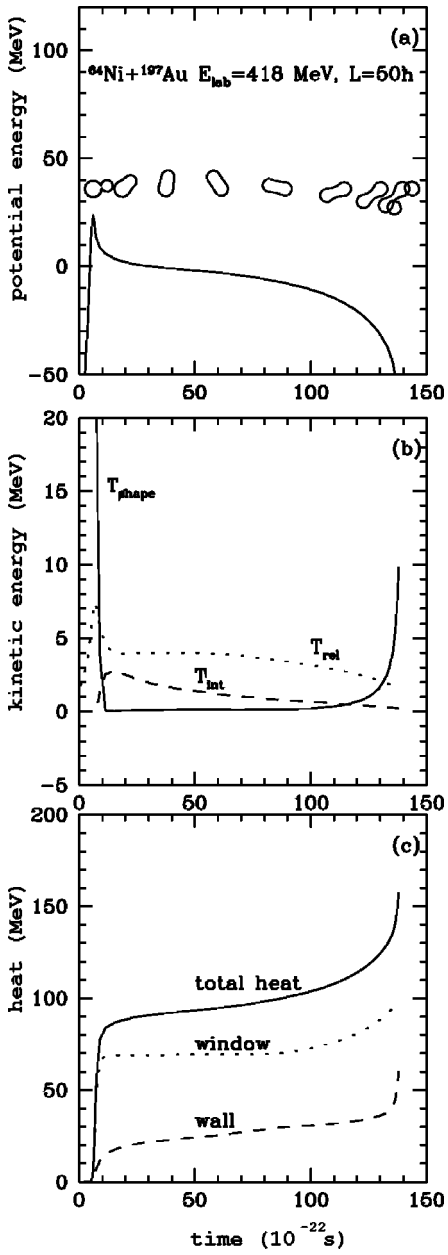

FIG. 6. Along the trajectory calculations: (a) potential energy and shapes. (b) Kinetic energy in the shape degrees of freedom $T_{\rm shape}$, relative rotation $T_{\rm rel}$, and intrinsic rotation $T_{\rm int}$. (c) Dissipated energy: total heat and the relative contributions from the window and wall dissipation.

2. HICOL calculations along the trajectory

A series of HICOL calculations was performed to investigate the dissipation mechanism responsible for the forward-backward asymmetry in the experimental angular distributions. The code implements a macroscopic description of dissipative heavy ion collisions [7]. A set of collective shape and angular coordinates is used and their evolution is followed, solving the equations of motion. The coupling of the macroscopic and the intrinsic degrees of freedom is considered explicitly in the derivation of the friction and the mass diffusion tensors, in which Fermi gas one-body formulas are used. A typical ''along-the-trajectory'' calculation, which will be used as an illustrative example, is shown in Fig. 6. We will consider a quasifission reaction of ^{64}Ni+^{197}Au at 418 MeV laboratory energy and initial orbital angular momentum $L=50\hbar$. The potential energy, the kinetic energy in the shape degrees of freedom $T_{\rm shape}$, in the angular degrees of freedom ($T_{\rm rel}$ and $T_{\rm int}$), and the dissipated energy are plotted as a function of time. In panel (a), the actual shapes along the trajectory are also shown. The trajectory starts at time $t=0$ when the nuclei are 14 fm apart. All the energy available to the system resides in kinetic energy of the shape and relative rotation. Within 6×10^{-22} s, the nuclei come into contact. At that time, the proximity friction has already produced about 8 MeV of heat. After the touching point, as the window opens, the radial motion is rapidly damped. With this, the shape loses most of its kinetic energy, since the other two shape coordinates—the neck and the asymmetry–do not possess any initial momentum. The viscous drag in the window sets into motion the intrinsic rotation. At $t=15\times10^{-22}$ s the window has produced 68 MeV of heat and is already widely open. At this point the shape changes from a necked-in to a convex type. The system enters the mononuclear regime, and a uniform wall is considered for the subsequent evolution. A long creeping motion with practically no kinetic energy in the shape follows. Without the window friction against the net particle flux, the asymmetry degree of freedom begins relaxing. It has been severely hindered up to now. As we move along the trajectory, the deformation develops again, the window comes back, and the total dissipation increases. The potential is rapidly falling, the system gains back kinetic energy in the shape (10 MeV in this case), and it scissions separating with final angular momentum $L_f=43\hbar$ and final fragment mass numbers $A_1=137$ and $A_2=124$. The TKE of the fragments is 221 MeV, consistent with our measurement and with Viola systematics. The mass variance is $\sigma^2_{AA}=888$ and the total number of exchanged particles through the window, $N_{\rm ex}=6614$. Within the reaction time of $\simeq140\times10^{-22}$ s the system does not complete one full rotation (the scattering angle is $-54°$). The fragment masses are correlated with the emission angles, which will result in asymmetric mass-angle distributions. This is a typical quasifission trajectory, with the system scissions bypassing the compound nucleus stage. The mass asymmetry is not fully relaxed, but almost all the initial kinetic energy is dissipated and the fragments fly apart driven by the strong Coulomb repulsion.

In the model implemented in HICOL, there are no free parameters. The only *ad hoc* procedure used is in the combination of window-plus-wall and monowall friction. For shapes with a ''fat'' neck, there is an ambiguity in the choice of a window plus two walls or a mononucleus shape without a window. To make a smooth transition between the two regions, a form factor $f(x_n)$ multiplying the rate of energy dissipation $\dot{Q}$ is introduced as follows:

$$\dot{Q}=[1-f(x_n)]\dot{Q}^{\rm win+wall}+f(x_n)\dot{Q}^{\rm mono}, \qquad (1)$$

with $x_n=R_{\rm neck}/\min(R_1,R_2)$ measuring the ratio between the neck radius and the radius of the smaller nucleus. For ''thin'' necks ($0<x_n<0.8$), $f(x_n)=0$ and the full window-plus-wall friction is used. In the region $0.8\leqslant x_n\leqslant1$, where the shape makes the dinucleus to mononucleus transition, $f(x_n)$ is smoothly rising from 0 to 1 and both window-plus-wall and monowall are used. For $x_n>1$, the energy dissipation is

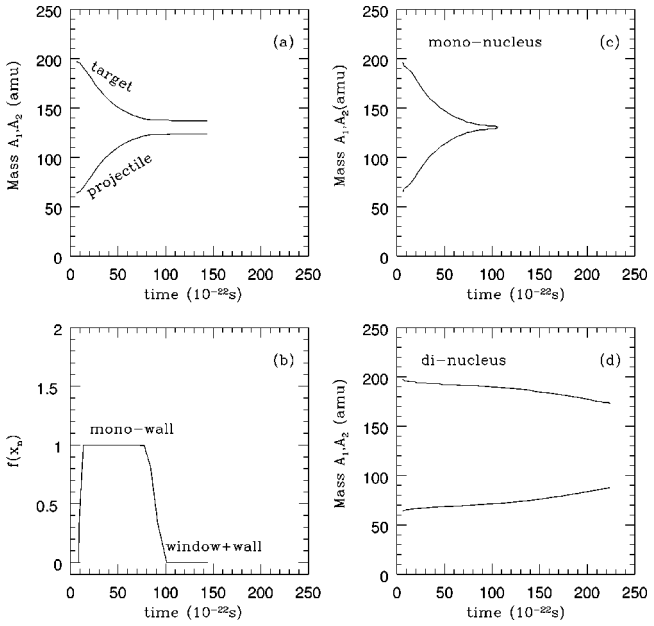

FIG. 7. Window-plus-wall or monowall? (a) The mass evolution of the projectilelike and the targetlike fragments is calculated for the $E_{\rm lab}=418$ MeV, $L=50\hbar$ trajectory with window-plus-wall and monowall friction mixed with a form factor $f(x_n)$ as described in the text. (b) The evolution of the form factor $f(x_n)$ along the same trajectory. (c) Fragment mass evolution calculated without the window friction [$f(x_n)=1$ along the whole trajectory independent of the shape] and (d) the mass evolution with $f(x_n)=0$, window-plus-wall everywhere.

calculated with the monowall formula. In the outgoing part of the trajectory, when the neck develops again, $f(x_n)$ drops from 1 to 0 after which, the full window-plus-wall friction is used until the scission point. The functional form of $f(x_n)$ and the limiting value $x_n=0.8$ are arbitrarily chosen. The concern when using such a description comes from the fact that the two formulas (window-plus-wall or monowall) give different results when applied to the same shape. The window-plus-wall formula can produce 4–8 times stronger friction against the mass-asymmetry equilibration than the wall formula alone. Figure 7(a) illustrates the mass evolution of the projectilelike and the targetlike fragment along the $E_{\rm lab}=418$ MeV, $L=50\,\hbar$ trajectory. The evolution of the form factor $f(x_n)$ is shown below it in Fig. 7(b). One can easily see that the main mass transfer from the target to the projectile happens during the mononucleus part of the trajectory, when the window friction is turned off. In Figs. 7(c) and 7(d) we have calculated the mass evolution in the two extreme cases: monowall friction along the whole trajectory or full window-plus-wall everywhere, respectively. Both these cases are clearly unphysical. Without the window friction, all trajectories proceed rather rapidly to symmetry, which is in contradiction with the experimental results (Sec. IV D) , while with the window-plus-wall acting everywhere, there are no trajectories that produce symmetric mass splits. In view of the above, we consider that the form factor $f(x_n)$ should be used as a free parameter and adjusted to match the experimental mass distributions.

In the dynamical analysis of the prescission neutron data of Hinde *et al.* [9], Wilczynski, Siwek-Wliczynska, and

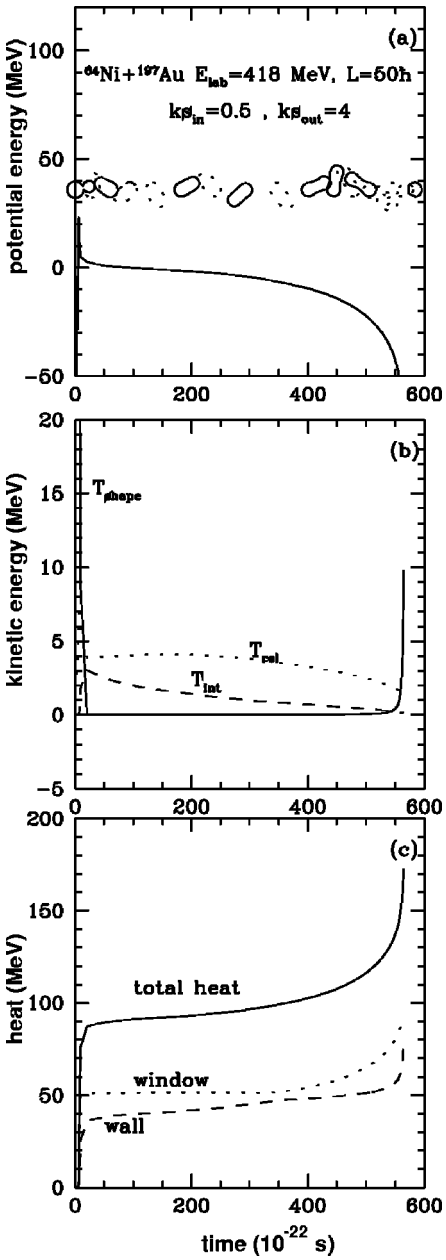

FIG. 8. As per Fig. 6 but calculated with large friction as in Ref. [11].

Wilschut [11] scaled the energy dissipation rate $\dot{Q}$ by an additional factor k_s, which was treated as a free parameter. The factor k_s was allowed to obtain values smaller than unity, when a reduction of the full one-body friction was needed, and $k_s>1$ was interpreted as evidence for two-body dissipation. Along the trajectory, the authors of Ref. [11] divided k_s into $k_s^{\rm in}$ and $k_s^{\rm out}$. In the early stage of the reaction, when the system is reasonably cold, a factor $k_s^{\rm in}=0.5$ was used, and after the mononucleus stage is reached and the system has converted a significant amount of kinetic energy into heat — $k_s^{\rm out}=4$–12 was applied to make the reaction time long enough to allow the emission of the requisite number of prescission neutrons. The justification for using such a description was the expected temperature dependence of nuclear viscosity.

Figure 8 shows the $L=50\hbar$ trajectory calculation

for ^{64}Ni+^{197}Au at $E_{\rm lab}=418$ MeV, which was done using $k_s^{\rm in}=0.5$ and $k_s^{\rm out}=4$ as described in Ref. [11]. The quantities plotted are the same as in Fig. 6 which was for the standard ($k_s=1$) HICOL trajectory. By comparing the two calculations one sees that the shape of the potential energy, kinetic energy, and total heat curves is similar, but the time scale is stretched in the large friction trajectory. The relative contributions from window and wall dissipation are different. By scaling down the friction in the early stage of the reaction when the window-plus-wall formula is used, the window contribution is reduced. Then, in the mononucleus stage, the weaker wall friction is scaled by a factor of 4. This brings the system into a relatively flat region of the potential with very little kinetic energy (mainly in rotation) and strong friction hindering its motion towards scission. It takes 3.5 times longer to develop the deformation and find its way to the steep slope of the potential that leads to scission. During this long reaction time, the system makes more than two full rotations, as seen in the shape evolution in the figure. The calculated final scattering angle is $-760°$. This will lead to orbiting type ($\sim 1/\sin\theta$) angular distribution of the fragments, instead of the asymmetric distribution expected from the trajectory in Fig. 6, which agrees qualitatively with the experimental results. The mass drift in the large-friction trajectory is similar to the one-body case, since the window friction was initially reduced ($k_s^{\rm in}=0.5$), and later increased, in the final part of the trajectory.

C. Cross sections

The experimental angular distributions were extrapolated to 0° and 180° as described by Back *et al.* in Ref. [20]. For fusion-fission reactions the angular distributions of the fragments are given by [21]

$$W(\theta)=\sum_{I=0}^{\infty}(2I+1)T_I \sum_{K=-I}^{I}\frac{\frac{1}{2}(2I+1)|d^I_{0K}(\theta)|^2\exp[-K^2/2K_0^2]}{\sum_{K=-I}^{I}\exp[-K^2/2K_0^2]}. \quad (2)$$

Here I is the total spin of the fissioning nucleus, K is the projection of I on the fission axis, T_I is the transmission coefficient for fusion of the Ith partial wave, and $d^I_{0K}(\theta)$ are the real parts of the Wigner D functions. Equation (2) gives angular distributions symmetric about 90° which approach the $1/\sin\theta$ classical distribution for $I\gg 0$. These are not applicable to describe the asymmetric angular distribution in short-time scale quasifission reactions. However, since a theoretical prescription for this type reactions is not available, Back *et al.* [20] used the following expression to fit the data from a measurement similar to the one done in this work:

$$\frac{d\sigma}{d\theta_{\rm c.m.}}=2\pi\sin\theta_{\rm c.m.}\exp[\beta(\theta_{\rm c.m.}-\pi/2)]W(\theta_{\rm c.m.}), \quad (3)$$

where β is the angular slope parameter. The same approach was adopted here. The transmission coefficients T_I were calculated using the extra-push estimate to the complete fusion cross section with a program due to Back [22]. The Wigner D functions for $I,K\leqslant 25$ were calculated using the CERN library routine DDJMNB, and the recursion relations [23] were used for larger spins. The value of K_0 was determined from the mass bin closest to symmetry, and kept fixed in the other mass bins. Best results were obtained with $K_0^2=25^{+25}_{-10}$ for the 418 MeV data and $K_0^2=15^{+20}_{-5}$ at 383 MeV. The overall normalization and the parameter β were varied to produce best fits to the data. In the systems studied by Back *et al.* [20] the clean separation of the quasifission and deep-inelastic events was possible, since the mass distributions were peaked at symmetry. In the case studied here, the mass distribution has a minimum at symmetry and these two reaction channels could not be separated (see also Fig. 2). The deep-inelastic scattering exhibits a maximum at the grazing angle of the reaction for A<80 (right panels in Figs. 4 and 5) and the above description of the angular distribution does not apply. The laboratory grazing angles for $E_{\rm lab}$418 MeV and 383 MeV are 55° and 65°, respectively. In order to fit the data, a Gaussian distribution was added to the distribution given in Eq. (3) and the relative contributions of the two distributions were adjusted to obtain agreement with the measurement. With this, an attempt was made to estimate the deep-inelastic and the capture cross sections separately. For the $A\geqslant 80$ mass bins (left panels in Figs. 4 and 5), the cross section is only due to capture reactions. The values for the total cross section measured, $\sigma_{\rm touch}=\sigma_{\rm DI}+\sigma_{\rm capture}$, and the estimated contributions from the two reaction channels are given in Figs. 4 and 5. The errors in $\sigma_{\rm touch}$, around 25%, come from the quality of the fits and the uncertainty in determining the monitor position and the detector solid angle ratios. The contribution from the statistical errors of the data is much smaller. The upper limit of the deep-inelastic cross section $\sigma_{\rm DI}$ was estimated with the assumption that for $A<80$ all the cross section forward of the grazing angle is in this channel. This brings the corresponding reduction in the capture cross section. The angle-integrated cross sections for the different mass bins are listed in Table II.

D. Mass distribution

After integrating the angular distributions in the different mass bins, the mass distributions for the two energies measured were obtained (see Fig. 9). At both energies, the distributions differ dramatically from the mass distributions of fusion-fission reactions, which are narrower and peaked at symmetry. This behavior can be qualitatively explained since, for this system which has fissility $x=0.915$, the symmetric saddle does not exist. The potential energy landscape always favors asymmetric mass division. Theoretical mass distributions were obtained using HICOL's predictions for the final mean fragment masses and their variances for each trajectory that leads to a damped reaction. A weighted sum over angular momentum was constructed, using the measured cross sections. The resulting mass distributions are plotted together with the experimental data in Fig. 9. The dashed-line histograms give the HICOL predicted mass distributions. Although the general trend of the data is reproduced, a quantitative agreement is not achieved. The code underpredicts the deep-inelastic scattering and overpredicts the yield at the

TABLE II. Angle-integrated cross sections in bins of 10 mass units from the two energies studied.

	$E_{lab}=418$ MeV			$E_{lab}=383$ MeV		
Mass (amu)	σ_c (mb)	σ_{DI} (mb)	σ_{touch} (mb)	σ_c (mb)	σ_{DI} (mb)	σ_{touch} (mb)
120–130	95 ± 21		95 ± 21	43 ± 10		43 ± 10
110–120	128 ± 29		128 ± 29	46 ± 11		46 ± 11
100–110	162 ± 37		162 ± 37	63 ± 15		63 ± 15
90–100	199 ± 45		199 ± 45	70 ± 16		70 ± 16
80–90	206 ± 47		206 ± 47	106 ± 24		106 ± 24
70–80	137^{+34}_{-68}	75^{+38}_{-19}	212 ± 59	62^{+15}_{-31}	62^{+31}_{-15}	124 ± 32
60–70	95^{+24}_{-48}	186^{+92}_{-46}	281 ± 79	50^{+12}_{-25}	194^{+97}_{-49}	245 ± 65
50–60	29^{+7}_{-15}	113^{+56}_{-28}	142 ± 40	$6.3^{+1.5}_{-3.1}$	134^{+67}_{-33}	140 ± 36
Total	1053^{+263}_{-350}	374^{+190}_{-93}	1427 ± 357	450^{+135}_{-194}	391^{+194}_{-117}	841 ± 210

symmetric mass division for both energies. Since the mass drift is governed by the window friction, and in HICOL the relative contributions of window-plus-wall and monowall friction are mixed with a form factor determined from the shape of the system along the trajectory, as discussed above, a variation of the form factor was considered in this work, in order to reproduce the experimental results. Allowing for the window friction to contribute for larger R_{neck} by changing the limits of x_n from $0.8\leqslant x_n\leqslant 1$ to $0.95\leqslant x_n\leqslant 1$ gave a satisfactory result for the 418 MeV data and a trend in the right direction for the 383 MeV data (the solid-line histograms in the figure). Further increase in the lower limit of x_n still did not reproduce the large deep-inelastic cross section measured at $E_{lab}=383$ MeV.

The discrepancy between HICOL and the data in the deep-inelastic channel was addressed by Feldmeier [7] and was attributed to the fact that the narrowly peaked phase space approximation is not strictly valid for the deep-inelastic trajectories. The mass variance is underpredicted in this region, which limits the partial waves that can contribute to the cross section in the near-projectile and target mass bins. Including fluctuations in the trajectory model will probably improve the agreement with the data. The code gives a reasonable description of the 418 MeV data, in which the deep-inelastic events comprise ≈1/4 of the total touch cross section. At the lower energy, where almost half of the touch cross section is in the deep-inelastic channel, only the shape of the distribution is reproduced by the calculations.

Comparison of the $E_{lab}=418$ MeV mass distribution data with other theoretical descriptions from the literature is presented in Fig. 10. In the work by Shen *et al.* [6], it was found that the full window-plus-wall dissipation gave reaction times which were too long and inconsistent with the time scales derived from the mass-angle correlations. The authors came to the conclusion that the window friction should not

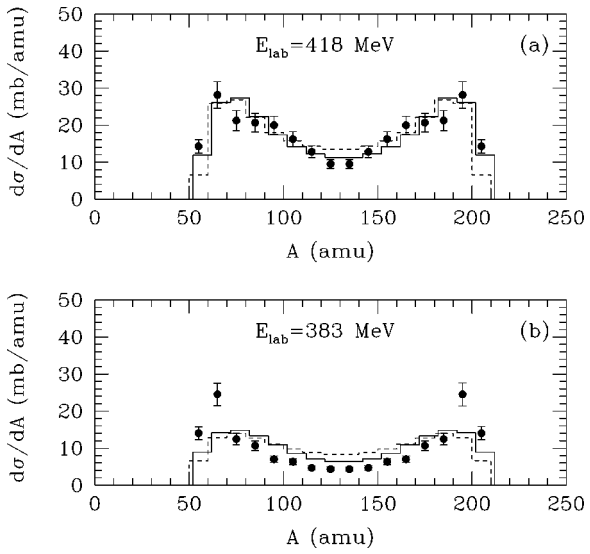

FIG. 9. Mass distributions: (a) $E_{lab}=418$ MeV and (b) $E_{lab}=383$ MeV. The data are shown with points. The histograms give HICOL calculations: dashed lines, unmodified HICOL; solid lines, the window-plus-wall to monowall form factor is modified as described in the text.

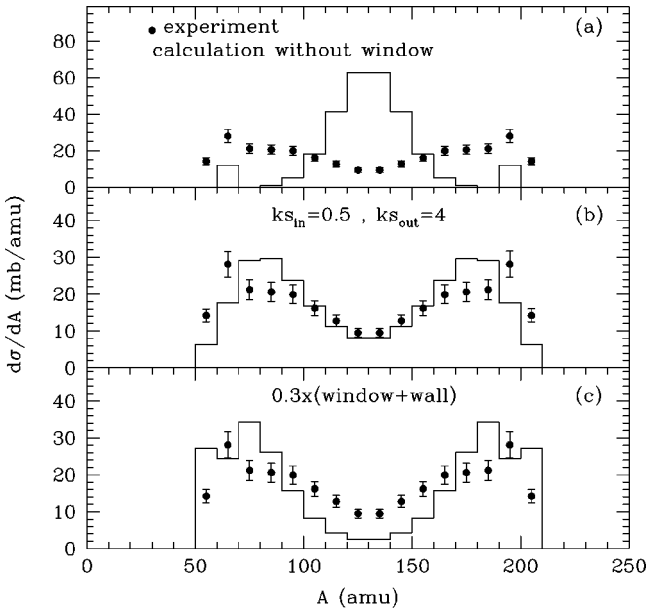

FIG. 10. Mass distribution calculations for $E_{lab}=418$ MeV in comparison to the data: (a) a calculation without the window friction, (b) a calculation with friction scaling according to Wilczynski, *et al.* [11], and (c) $0.3\times$(window+wall) along the whole trajectory.

be included in the calculation.

In Fig. 10(a), a calculation without the window friction is presented. It differs dramatically from the data, since the window friction is the main mechanism that prevents the fast equilibration of the mass asymmetry. Figure 10(b) shows a calculation done using a prescription of Wilczynski *et al.* [11] for scaling the friction along the trajectory, which was already discussed in Sec. IV B 2. Although this calculation reproduces the mass distribution, it does not reproduce the mass-angle correlations, since the reaction times are longer than the rotational period of the system (see Sec. IV B 2).

A frequently used approach to implement friction in various descriptions of heavy ion reactions is to use window-plus-wall dissipation during the whole reaction, but scaled by a factor of ≈ 0.3, which was determined from fitting experimental fission fragment TKE distributions and giant resonance widths [24]. Figure 10(c) shows the calculated mass distribution using this approach, in comparison to the 418 MeV data. With the window friction present during the whole trajectory, even if it is scaled down, the mass drift towards symmetry is hindered significantly resulting in disagreement with the data.

Using a shape dependent friction along the whole trajectory, as was done in HICOL, reproduces in a self-consistent way the mass distributions [Fig. 9(a)], the mass-angle correlations (Figs. 4 and 11) and the fission fragment TKE. The other approaches discussed here fail to reproduce all observables at once. There are minor discrepancies between the model and the experimental results which show that the form factor mixing window-plus-wall and monowall friction requires further investigation. The mass variances for the deep-inelastic trajectories also need further refinements in order to yield better agreement with the experimentally measured cross sections.

E. Mass-angle correlations and reaction times

From the measured angular distributions extrapolated to 0° and 180°, the double differential cross sections $d^2\sigma/(d\theta_{\mathrm{c.m.}}dA)$ were constructed.

The results are plotted in Fig. 11. The contour levels are listed in the figure. A forward-backward asymmetry, which reveals the short-time scale of the reaction, is clearly evident for both energies measured. A two-body friction mechanism with $1/T^2$ temperature dependence, as suggested in Ref. [11], would require friction scaling factors of $k_s^{\mathrm{out}}=10-12$ for $E_{\mathrm{lab}}=383$ MeV and $k_s^{\mathrm{out}}=4$ for the higher energy, which in both cases results in time scale much longer than the rotational period of the system and flat $d\sigma/d\theta_{\mathrm{c.m.}}$ distributions. Only the deep-inelastic component of the *touch* cross section would retain the asymmetry about $\theta_{\mathrm{c.m.}}=90°$. Since the data do not show this behavior, the large-friction scenario is *ruled out*. A direct comparison of the measured double differential cross sections $d^2\sigma/(d\theta_{\mathrm{c.m.}}dA)$ and HICOL could not be done, since the code predicts the mean value of the scattering angle, but does not calculate its variance.

For all partial waves, the calculated mean scattering angles are smaller than 180°, which is consistent with the experimental observation of a nonorbiting angular distribution. Although HICOL suggests the correct behavior, there is an indication that the reaction times for the intermediate

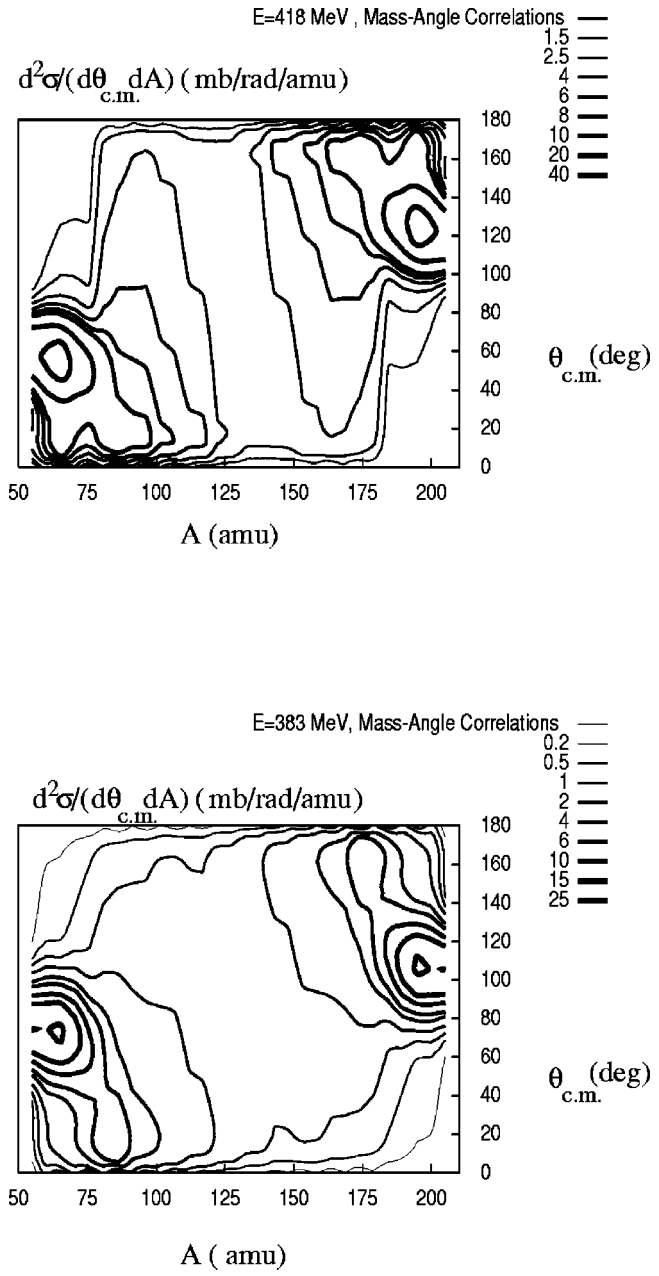

FIG. 11. Double differential cross sections $d^2\sigma/(d\theta_{\mathrm{c.m.}}dA)$ (mb/rad/amu) from the two energies measured. The contour levels are shown in the plots.

masses are overpredicted, since in the experiment all fragments in this range are peaked forward with a maximum yield angle in the vicinity of 20° and an average angle of 60°–80°. A larger saturation angle ($\approx 100°$) is obtained from the calculation. The correct description of the measured angular distributions would require a considerable dispersion around the mean values, which is not calculated by HICOL, and mean angles smaller by $\approx 30°$.

An upper limit to the reaction time can be estimated using the characteristic rotational time of the system for the longest lasting trajectories. At $E_{\mathrm{lab}}=418$ MeV, for the average quasifission trajectory, contributing in the symmetric mass bin $A=120-140$, $L=46\hbar$, and moment of inertia of two touching spheres we estimate $\tau \sim 30\times 10^{-21}$ s. In HICOL, the rotational frequency and the moment of inertia are changing

TABLE III. Reaction times for the average quasifission trajectories contributing in the $A=120-140$ mass range.

$E_{\rm lab}$ (MeV)	$\langle L\rangle\ \hbar$	time$\times 10^{-21}$ s
418	46	15
383	22	16

along the trajectory and reflect the evolution of the shape and rotational degrees of freedom. HICOL's result for the same trajectory is $\tau=15\times10^{-21}$ s, which is in excellent agreement with the time extracted from the neutron measurement, $\tau=18\pm9\times10^{-21}$ s [9]. In contrast the calculation [10] of Siwek-Wilczynska *et al.* extracted $\tau=80^{+55}_{-25}\times10^{-21}$ s from the same data. Table III gives the HICOL results obtained for the average trajectories contributing in symmetric quasifission for the two energies measured.

The two completely different physics approaches of Ref. [9] and this work have yielded similar results for the reaction time scale, which indicates that the one-body friction implemented in HICOL gives a satisfactory description of the reaction mechanism. However, a dynamical calculation of the prescission particle emission is necessary, in order to relate the prescission neutron multiplicity to the viscosity. Such calculations were done in this work and are presented in the Appendix. After adjusting the statistical model parameters, so that both the measured prescission neutron multiplicities and mean neutron kinetic energies are reproduced, the time scale derived from our dynamical calculation is in agreement with the original ''static'' results of Ref. [9].

V. ONE-BODY DISSIPATION LIMITS

To determine the experimental limits to the one-body viscosity, implemented in HICOL, calculations were done using scaling factors to the friction tensor ranging from $k_s=0.5$ to $k_s=4$ and tested versus the experimental mass and angular distributions. These factors were kept constant along the whole trajectory, thus preserving the original shape dependence of friction, which would be destroyed if different scaling factors were used in different parts of the trajectory.

Figure 12 shows the results for $k_s=1.7$ and $k_s=0.8$, which we determine as the limits beyond which the calculations are in considerable disagreement with the data. Scaling factors $k_s\geqslant1.7$ lead to scattering angles $\geqslant180°$ [Fig. 12(b)] and orbiting-type angular distributions, which are inconsistent with the data (see also Figs. 4 and 11). The mean experimental angles in Fig. 12(b) were determined using the fits to the angular distributions in Fig. 4 and plotted as points in the middle of the corresponding mass bins. The errors were derived from the quality of the fits. In the lower limit, $k_s\leqslant0.8$, although the mean scattering angles are in agreement with the experiment, there is considerable discrepancy between the calculated and the measured mass distributions [Fig. 12(a)]. This analysis sets the upper and lower limits to the one-body friction scaling factors for the temperature range of the quasifission reactions studied in this work. The two measurements in the present study cover the temperature range of the prescission neutron data from Ref. [9]. In contrast to the calculations in Ref. [11] which found that scaling factors $k_s=4-12$, varying with temperature, were needed to

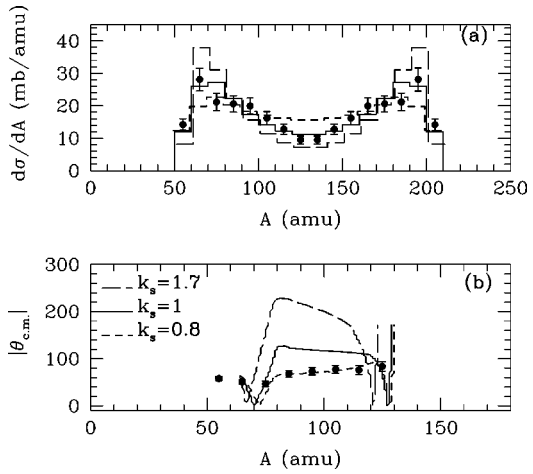

FIG. 12. Mass distributions (a) and mean scattering angles (b) calculated with HICOL with scaling factors: $ks=1.7$, long-dashed histograms and curves; $ks=0.8$, short-dashed histograms and curves; $ks=1$, solid lines. The experimental data for $E_{\rm lab}=418$ MeV are shown with points.

describe the data in Ref. [9], we consider both our measurements are consistent with one-body viscosity. Supporting this conclusion, Feldmeier in [7] analyzed the ^{238}U+^{48}Ca at $E_{\rm lab}=5.9$ MeV/nucleon data from Shen *et al.* [6], and reproduced the measured mass distributions with his code. A prescission giant dipole resonance GDR γ-ray measurement and analysis [25] in the quasifission reaction of ^{58}Ni $+^{165}$Ho at $E_{\rm lab}=368$ MeV was also consistent with one-body friction.

There have been a number of studies in fusion-fission and fusion-evaporation reactions based on the statistical model, which show the need for dissipation in the fission degree of freedom. Systematic studies by the Stony Brook group (see Ref. [12] and references therein) on prescission GDR γ rays indicates that viscosity increases with temperature and is larger than the one-body value. Some of these results were used in Ref. [11] and together with the prescission neutron multiplicity calculations discussed above were interpreted as evidence for two-body viscosity setting in at temperature $T\leqslant2$ MeV.

On the other hand, other studies from prescission particle multiplicities (e.g., Refs. [26,27]) and GDR γ rays (e.g., Ref. [28]) in the same temperature range do not find evidence for such large viscosity. A recent measurement of Morton *et al.* [29] of GDR γ-ray multiplicities for the ^{32}S+ $^{\rm nat}$W, ^{208}Pb reactions also found a delay time consistent with one-body dissipation and γ-fission angular correlations that could be described without temperature dependent viscosity. At present, the dissipation mechanisms in fusion-fission reactions and the temperature at which the two-body dissipation sets in is still a subject of considerable debate.

VI. CONCLUSIONS

The present study concentrated on the quasifission reaction dynamics, exploiting the unique observables available in this type of reactions: mass-angle correlations and mass distributions. It aimed to clarify and reconcile the data and the theoretical descriptions of nuclear viscosity that were avail-

able prior to this. We find that two different experimental observables — mass-angle correlations, and prescission neutron multiplicities — have yielded similar results. Our data analysis in terms of the one-body dissipation theory was qualitatively successful. The reaction times obtained from this study were in very good agreement with the results deduced from prescission neutron multiplicities using a completely different physics approach. Our own dynamical evaporation calculation with the code DIFHEAT was performed for the neutron data (see the Appendix) and reconciled with the original statistical model analysis of Hinde *et al.* In this work it was shown how the mass distributions by themselves are also sensitive to the dissipation mechanism. The new results do not confirm the onset of two-body viscosity in the temperature range below $T=2.5$ MeV.

ACKNOWLEDGMENTS

The authors would like to express their gratitude to the staff at the Nuclear Structure Laboratory in Stony Brook for their continuous support. The targets were skillfully prepared by A. Lipski. Fruitful discussions with P. Paul, B.B. Back, and H.W. Wilschut are gratefully acknowledged. This work was sponsored in part by the U.S. National Science Foundation. I.D. acknowledges the support of the OTKA Foundation, Grant No. 017285.

APPENDIX: HICOL PLUS EVAPORATION

In the approach of Siwek-Wilczynska *et al.* [10], HICOL's trajectory was divided into time steps. A statistical model calculation was applied for each step, replacing the excitation energy with HICOL's dissipated energy minus the energy lost in evaporation from the previous step.

A similar code was developed independently in this work using a somewhat different approach. Instead of dividing the trajectory into time steps, a continuous evaporation process was assumed, following Refs. [30,31]. The results of Refs. [10,11] could be reproduced with our code DIFHEAT.

Calculating the accumulated neutron multiplicity along the $L=40\hbar$ trajectory in $^{64}Ni+^{197}$Au at $E_{\rm lab}=418$ MeV, using a level density parameter $a=A/9$ MeV^{-1} (the value used in the neutron measurement), one finds that the calculated prescission multiplicity does not reach the experimental value. In Refs. [10,11], the authors concluded that the reaction time predicted by HICOL using one-body friction is too short to be able to accommodate the measured prescission neutron multiplicities.

A different approach to reconcile the measured prescission neutron multiplicity with the dynamical trajectory calculation was applied in this work. It appears that the discrepancy between the calculations of Hinde *et al.* [9] and Wilczynski's *et al.* [10,11] does not stem from the ''static'' versus ''dynamical'' approach, but rather reflects the different nuclear temperature achieved in the two cases. In the calculation of Hinde *et al.* the level density parameter was kept fixed at the value $a=A/9$ MeV^{-1}, but the excitation energy of the system was treated as a free parameter[1] and adjusted in order to reproduce *both* the measured prescission neutron multiplicity and spectral shapes. Although routinely in statistical model calculations the level density parameter is varied, while the excitation energy is fixed, as Hinde *et al.* pointed out, both observables are sensitive to the nuclear temperature $T=\sqrt{E^*/a}$, which contains the ratio of the two quantities. The authors of Ref. [10] argued that the dynamically calculated excitation energy, as predicted by HICOL[2] should be used. Keeping the level density parameter at the same value of $a=A/9$ MeV^{-1}, but using a lower excitation energy along the trajectory ($E^*\sim 100$ MeV), results in a lower nuclear temperature. Consequently, this calculation yields longer neutron lifetimes and, in addition, *does not* reproduce the mean neutron kinetic energy.

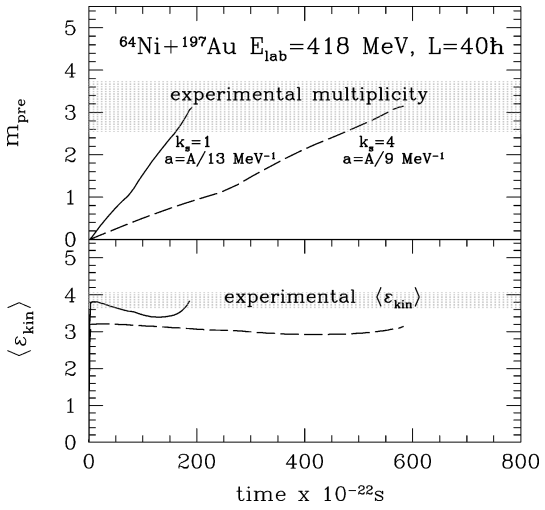

FIG. 13. Prescission neutron multiplicity and mean neutron kinetic energy along the trajectory.

The dashed curves in Fig. 13 show the neutron multiplicity and the mean neutron kinetic energy along the trajectory, calculated with $a=A/9$ MeV^{-1} and an input heat curve obtained by scaling the friction in HICOL by a factor $k_s=4$. The shaded regions indicate the experimental multiplicity and mean kinetic energy values reported in Ref. [9].

Since HICOL indeed provides a more consistent description of the excitation energy, than the fitting procedure used in Ref. [9], in order to produce the same temperature ($T\approx 2.2$ MeV), as derived from the neutron spectra measured by Hinde *et al.*, we need to vary the level density parameter. From Fig. 6(c) we find that $E^*\approx 100$ MeV, and we estimate that $a=A/12.7$ MeV^{-1} should reproduce *both* the neutron lifetimes and mean kinetic energy. The solid lines in Fig. 13 show the result from DIFHEAT, using a level density parameter $a=A/13$ MeV^{-1} and a one-body dissipation heat curve coming from HICOL.

Unlike the conclusion in Ref. [11] that large friction is necessary to reproduce the experimental prescission neutron

[1] $E^*=E_x+\Delta E_x$. $E_x=95.3$ MeV was determined from the Q value of the reaction and $\Delta E_x=50$ MeV was obtained from the fit to the data.

[2] See the total heat curve in Fig. 6(c).

multiplicities—we find that the reaction time extracted from the neutron data, $\sim 20\times 10^{-21}$ s is consistent with HICOL's predictions and with the evaporation calculation using DIFHEAT, if the statistical model parameters are properly constrained. While HICOL is free of adjustable parameters, in any statistical model calculation one needs at least two observables, to be able to constrain the multiparameter model calculation. It is beyond the scope of this work to investigate the influence of all statistical model parameters on the results from DIFHEAT. There is a significant deformation dependence both in the particle transmission coefficients and their binding energies [32,26]. Accounting for these effects might change the value of the level density parameter needed to describe the data. However, we note that values as small as $a\sim A/13$ MeV^{-1} have been previously deduced from particle spectral shapes in heavy hot systems [33,34].

[1] J. R. Huizenga and W. U. Schröder. in *Semiclassical Descriptions of Atomic and Nuclear Collisions* (Elsevier, Amsterdam, 1985), p. 255.

[2] W. U. Schröder and J. R. Huizenga, in *Treatise of Heavy-Ion Science* (Plenum Press, New York, 1984), Vol. 2.

[3] B.B. Back, R.R. Betts, J.E. Gindler, B.D. Wilkins, S. Sinai, M.B. Tsang, C.K. Gelbke, W.G. Lynch, M.A. McMahan, and P.A. Baisden, Phys. Rev. C **32**, 195 (1985).

[4] J. Tõke, R. Bock, A. Gobbi, S. Gralla, K.D. Hildenbrand, J. Kuzminski, W.F.J. Müller, A. Olmi, H. Stelzer, B.B. Back, and S. Bjørnholm, Nucl. Phys. **A440**, 327 (1985).

[5] R. Bock, Y.T. Chu, M. Dakowski, A. Gobbi, E. Grosse, A. Olmi, H. Sann, D. Schwalm, U. Lynen, W. Müller, S. Bjørnholm, H. Esbensen, W. Wölfli, and E. Morenzoni, Nucl. Phys. **A388**, 334 (1982).

[6] W.Q. Shen, J. Albinski, A. Gobbi, S. Gralla, K.D. Hildenbrand, N. Herrmann, J. Kuzminski, W.F.J. Müller, H. Stelzer, J. Tõke, B.B. Back, S. Bjørnholm, and S.P. Sørensen, Phys. Rev. C **36**, 115 (1987).

[7] H. T. Feldmeier, ''Dissipative Heavy-Ion Collisions,'' Argonne National Laboratory, Report No. ANL-PHY-85-2, 1985.

[8] D.J. Hinde, D. Hilscher, and H. Rossner, Nucl. Phys. **A502**, 497c (1989).

[9] D.J. Hinde, D. Hilscher, H. Rossner, B. Gebauer, M. Lehmann, and M. Wilpert, Phys. Rev. C **45**, 1229 (1992).

[10] K. Siwek-Wilczynska, J. Wilczynski, R.H. Siemssen, and H.W. Wilschut, Phys. Rev. C **51**, 2054 (1995).

[11] J. Wilczynski, K. Siwek-Wilczynska, and H.W. Wilschut, Phys. Rev. C **54**, 325 (1996).

[12] D.J. Hofman, B.B. Back, and P. Paul, Phys. Rev. C **51**, 2597 (1995).

[13] R. Butsch, D.J. Hofman, C.M. Montoya, P. Paul, and M. Thoennessen, Phys. Rev. C **44**, 1515 (1991).

[14] N. Carjan, A.J. Sierk, and J.R. Nix, Nucl. Phys. **A452**, 381 (1986).

[15] J. Blocki, R. Planeta, J. Brzychczyk, and K. Grotowski, Z. Phys. A **341**, 307 (1992).

[16] D. Boilley, E. Suraud, Y. Abe, and S. Ayik, Nucl. Phys. **A556**, 67 (1993).

[17] W. Bohne, W. Galster, K. Grabishc, and H. Morgenstern, Nucl. Instrum. Methods Phys. Res. A **240**, 145 (1985).

[18] M. Ogihara, Y. Nagashima, W. Galster, and T. Mikumo, Nucl. Instrum. Methods Phys. Res. A **251**, 313 (1986).

[19] J. Velkovska and R.L. McGrath, Nucl. Instrum. Methods Phys. Res. A (to be published), nucl-ex/9807008.

[20] B.B. Back, P.B. Fernandez, B.G. Glagola, D. Henderson, S. Kaufman, J.G. Keller, S.J. Sanders, F. Videbæk, T.F. Wang, and B.D. Wilkins, Phys. Rev. C **53**, 1734 (1996).

[21] R. Vandenbosch and J. R. Huizenga, *Nuclear Fission* (Academic Press, New York, 1973).

[22] B. B. Back (private communication).

[23] D. A. Varshalovich, A. N. Moskalev, and V. K. Khersonskii, *Quantum Theory of Angular Momentum* (World Scientific, Singapore, 1988).

[24] J. R. Nix and A. J. Sierk, Los Alamos National Laboratory, Report No. LA-UR-87-133, 1987.

[25] J. Nestler, B.B. Back, K.S. Drese, D.J. Hofman, S. Schadmand, R. Varma, and P. Paul, Phys. Rev. C **51**, 2218 (1995).

[26] J.P. Lestone, Phys. Rev. Lett. **70**, 2245 (1993).

[27] J.P. Lestone, ''Ninth Winter Workshop on Nuclear Dynamics,'' Key West, 1993.

[28] G. van 't Hof, J.C.S. Bacelar, I. Dioszegi, M.N. Harakeh, W.H.A. Hesselink, N. Kalantar-Nayestanaki, A. Kugler, H. van der Ploeg, A.J.M. Plompen, and J.P.S. van Schagen, Nucl. Phys. **A599**, 17c (1996).

[29] C.R. Morton, A. Buda, P. Paul, N.P. Shaw, J.R. Been, N. Gan, M.L. Halbert, D.W. Stracener, R.L. Varner, M. Thoennessen, P. Thirolf, and I. Diòszegi, J. Phys. G **23**, 1383 (1997).

[30] R.J. Charity, R. Freifelder, A. Gobbi, N. Herrmann, K.D. Hildenbrand, F. Rami, H. Stelzer, J.P. Wessels, G. Casini, P.R. Maurenzig, A. Olmi, A.A. Stefanini, J. Galin, D. Guerreau, U. Jahnke, A. Peghaire, J.C. Adolff, B. Bilwes, R. Bilwes, G. Rudolf, M. Petrovici, M. Gnirs, and D. Pelte, Z. Phys. A **341**, 53 (1991).

[31] H. Delagrange, C. Grégoire, and F. Scheuter, Z. Phys. A **323**, 437 (1986).

[32] J.P. Lestone, J.R. Leigh, J.O. Newton, D.J. Hinde, J.X. Wei, J.X. Chen, S. Elfstrom, and D.G. Popescu, Phys. Rev. Lett. **67**, 1078 (1991),

[33] B.J. Fineman, K.-T. Brinkmann, A. L. Caraley, N. Gan, R.L. McGrath, and J. Velkovska, Phys. Rev. C **50**, 1991 (1994).

[34] B. J. Fineman, Ph.D. thesis, State University of New York at Stony Brook, 1994.